

# Evidence for outflows in $z \sim 6$ galaxies with ALMA

S. Gallerani<sup>1\*</sup>, A. Pallottini<sup>1,2</sup>, C. Feruglio<sup>1</sup>, A. Ferrara<sup>1</sup>, R. Maiolino<sup>2,3</sup>, L. Vallini<sup>4,5</sup>,  
D. A. Riechers<sup>6</sup>

<sup>1</sup> *Scuola Normale Superiore, Piazza dei Cavalieri 7, 56126, Pisa, Italy*

<sup>2</sup> *Kavli Institute for Cosmology, University of Cambridge, Madingley Road, Cambridge CB3 0HA, United Kingdom*

<sup>3</sup> *Cavendish Laboratory, University of Cambridge, 19 J. J. Thomson Ave., Cambridge CB3 0HE, United Kingdom*

<sup>4</sup> *Dipartimento di Fisica e Astronomia, Università di Bologna, viale Berti Pichat 6/2, 40127 Bologna, Italy*

<sup>5</sup> *Istituto Nazionale di Astrofisica - Osservatorio Astronomico di Bologna, via Ranzani 1, I-40127 Bologna, Italy*

<sup>6</sup> *Department of Astronomy, Cornell University, 220 Space Sciences Building, Ithaca, NY 14853, USA*

\* *To whom correspondence should be addressed; E-mail: simona.gallerani@sns.it*

9 December 2024

## ABSTRACT

We present the first attempt to detect outflows from galaxies approaching the Epoch of Reionization (EoR) using a sample of 9 star-forming ( $5 \lesssim \text{SFR} \lesssim 70 \text{ M}_\odot \text{ yr}^{-1}$ )  $z \sim 6$  galaxies for which high-quality spectra of the [CII]158 $\mu\text{m}$  line has been previously obtained with ALMA. We first fit each line with a Gaussian function and compute the residuals by subtracting the best fitting model from the data. We combine the residuals of all sample galaxies and find that the total signal is characterized by a flux excess that can be ascribed to broad wings of the [CII] line, which we interpret as a signature of starburst-driven outflows. The tentatively inferred outflow rate is  $\dot{M} \sim 65 \text{ M}_\odot \text{ yr}^{-1}$ . Our interpretation is consistent with results from zoomed hydro-simulations of *Dahlia*, a  $z \sim 7$  galaxy ( $\text{SFR} \sim 100 \text{ M}_\odot \text{ yr}^{-1}$ ) whose feedback-regulated star formation results in an outflow rate  $\dot{M} \sim 30 \text{ M}_\odot \text{ yr}^{-1}$ . These results suggest that starburst-driven outflows are in place in the EoR. Deeper observations of the [CII] line in the galaxies of this sample are required to better characterize stellar feedback at high- $z$  and to understand the role of outflows in shaping early galaxy formation.

**Key words:** galaxies: ISM - galaxies: evolution - galaxies: high-redshift

## 1 INTRODUCTION

Massive stars profoundly affect the interstellar medium of galaxies by injecting energy and momentum in the gas. This occurs via radiation pressure, stellar winds, photoionization, and supernovae (Dekel & Silk 1986; Mac Low & Ferrara 1999; Murray et al. 2011). As a result the gas is heated and ionized, and it becomes turbulent. Moreover, a substantial fraction of the interstellar medium (ISM) can be cast into the halo (Hopkins et al. 2012) and the intergalactic medium (IGM), thus enriching these components with freshly produced heavy elements (Oppenheimer & Davé 2006; Pallottini et al. 2014). Outflows also play a key role in the life-cycle of galaxies, as they control star formation by regulating the amount of gas available to form stars. On cosmological scales, outflows are thought to shape the faint-end of the galaxy luminosity function up to the highest redshifts at which galaxies can be observed (Bouwens et al. 2014; Dunlop 2013). This complex network of physical processes is collectively known as “feedback”.

Theoretically, modeling feedback represents a

formidable challenge. This is because its ab-initio implementation in cosmological simulations is hampered by the range of scales (from Mpc to sub-pc; Agertz et al. 2013) involved in the problem, and also by the complexity of the physical network. Nevertheless, some simple scalings with global properties of galaxies have provided at least a phenomenological link to observations (Davé et al. 2012; Dayal et al. 2014).

Observations provide crucial insights and guidance into outflow physics and driving. The most studied local starburst galaxy, M82, shows a prominent biconical, multiphase outflow. X-ray observations imply the coexistence of tens of millions-degree gas together with warmer H $\alpha$ -emitting phase (Lehnert et al. 1999) in which cold, molecular clumps are embedded, as revealed by CO observations (Walter et al. 2002). Evidence of outflows from local dwarf galaxies are also abundant (e.g. Martin, Kobulnicky & Heckman 2002; see also review by Veilleux, Cecil & Bland-Hawthorn 2005). Finally, very fast (up to 1000-2000 km/s) molecular gas, extending on kpc scales has been found in a few dozen systems,

arXiv:1604.05714v1 [astro-ph.GA] 19 Apr 2016

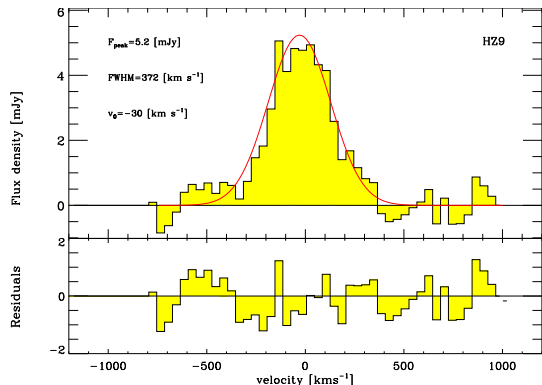


**Figure 1.** **Top panel:** [CII] emission line observed in the galaxy HZ9 by Capak et al. (2015) (yellow histogram). The red solid line represents the gaussian fit to the data. The best fit parameters (FWHM,  $F_{\text{peak}}$ ,  $v_0$ ) are reported. **Bottom panel:** The normalized residual,  $R$ , is shown with a yellow shaded histogram; the standard normal deviate,  $G$ , by a gray hatched histogram.

mostly highly obscured AGN in dusty star forming galaxies (Feruglio et al. 2015; Cicone et al. 2014; Veilleux et al. 2013)

At higher redshifts, detecting outflows becomes much more difficult. However, thanks mostly to absorption line spectroscopy, the presence of powerful outflows in galaxies close to the peak of the cosmic star formation ( $z \approx 2 - 3$ ), has been firmly assessed (Shapley et al. 2003; Steidel et al. 2010). Pushing observations into the Epoch of Reionization (EoR,  $z > 6$ ) is clearly the next frontier. This would be particularly important for several reasons. First, quasar absorption line experiments have shown that the IGM is already substantially enriched by the end of the EoR (D’Odorico et al. 2013), thus bringing a strong argument in favor of widespread galactic outflow activity. Second, a consensus exists that reionization has been primarily driven by ionizing photons produced low-mass galaxies (Choudhury & Ferrara 2007; Finkelstein et al. 2012; Mitra et al. 2012; Robertson et al. 2015; Mitra et al. 2015; Bouwens et al. 2015) which are the most sensitive to feedback effects. Thus, outflows have likely regulated the reionization process both by modulating star formation, and the escape of LyC photons through the resulting hot cavities.

In this paper we present the first attempt to use ALMA data to detect outflows from galaxies in the EoR. Specifically, we concentrate on a recently studied (Capak et al. 2015, hereafter C15) sample of 9 star forming galaxies ( $5 \lesssim \text{SFR} \lesssim 70 M_{\odot} \text{ yr}^{-1}$ ) at high- $z$  ( $5.2 \lesssim z \lesssim 5.7$ ), characterized by stellar masses  $\sim 10^{10} M_{\odot}$  for which high-quality spectra of the [CII]158 $\mu\text{m}$  line has been obtained. Encouraged by the success in detecting outflows from high- $z$  quasars using sub-mm lines (Maiolino et al. 2012; Cicone et al. 2015), we have refined such technique and applied it to the C15 sample<sup>1</sup>. In the following, we report the first tentative evidence of outflows in galaxies less than a billion years from the Big Bang.

## 2 METHOD

For each galaxy in the C15 sample, we fit the [CII] emission line ( $F_{\text{obs}}$ ) with a Gaussian function ( $F_{\text{mod}}$ ), whose free parameters are the full width at half maximum, FWHM, the peak flux,  $F_{\text{peak}}$ , and the center velocity,  $v_0$ . Moreover, we quantify the noise ( $\sigma_n$ ) of the spectrum by computing the standard deviation of the observed flux in pixels characterized by a velocity  $|v| > v_{\text{cont}}$ , where<sup>2</sup>  $v_{\text{cont}} = 700 \text{ km s}^{-1}$ . Finally, we compute the residuals by subtracting the best fitting model from the observed spectrum, and normalize them to the noise,  $R = (F_{\text{obs}} - F_{\text{mod}})\sigma_n^{-1}$ . For each galaxy, we also compute a *standard normal deviate*<sup>3</sup>, hereafter called  $G$ . As an example, in Fig. 1 we show the results from the above procedure for HZ9, the galaxy in the sample that is detected at the highest signal-to-noise ratio.

We then combine both  $R$  and  $G$  of all galaxies into single arrays:

$$R^{\text{tot}}(v) = \frac{1}{n_{\text{gal}}} \sum_{j=1}^{n_{\text{gal}}} R^j(v); G^{\text{tot}}(v) = \frac{1}{n_{\text{gal}}} \sum_{j=1}^{n_{\text{gal}}} G^j(v). \quad (1)$$

The final signal  $R^{\text{tot}}$ , rebinned to  $100 \text{ km s}^{-1}$ , and multiplied for the mean noise of all galaxies ( $\bar{\sigma} \sim 0.7 \text{ mJy}$ ) is shown in Fig. 2, where we have differentiated pixels characterized by  $|v| > v_{\text{cont}}$ , from those with  $|v| < v_{\text{cont}}$ . In the same figure, we plot  $G^{\text{tot}}$  with an hatched gray region, rebinned as  $R^{\text{tot}}$ , and  $R^{\text{tot}} \times \bar{\sigma}$  with a solid black line at a resolution of  $20 \text{ km s}^{-1}$ . Both in individual sources and in the stacked spectrum, the analysis takes into account the removal of a residual continuum term due to faint, individually undetected continuum or residuals in the subtraction.

If the observed spectra were completely determined by a single Gaussian [CII] emission line, the flux density of  $R^{\text{tot}}$  should consist simply of noise. In other words, both  $R^{\text{tot}}$  and  $G^{\text{tot}}$  should be described, by construction, by a *standard normal deviate*. We compute the cumulative distribution function (CDF) both of  $R^{\text{tot}}$  and  $G^{\text{tot}}$ , at a resolution of  $20 \text{ km s}^{-1}$ , and we compare them with the error function:

$$\text{erf}(x) = \frac{2}{\sqrt{\pi}} \int_0^x e^{-t^2} dt, \quad (2)$$

that describes the CDF of a *standard normal deviate*. The resulting CDFs of  $R^{\text{tot}}$  (solid black line) and  $G^{\text{tot}}$  (dashed black line) are shown in Fig. 3, where the solid black line denotes the CDF of  $R^{\text{tot}}$  and the dashed black line the CDF of  $G^{\text{tot}}$ . The blue and magenta lines show the CDF of  $R^{\text{tot}}$  for  $|v| > v_{\text{cont}}$  and  $|v| < v_{\text{cont}}$ , respectively, while the gray-shaded region is the result of the CDFs computed for 500 *standard normal deviates*. Finally, the dotted line represents the CDF described by eq. 2. The CDF of  $G^{\text{tot}}$  is, as expected, well within the gray-shaded regions. Interestingly, the CDF of  $R^{\text{tot}}$  strongly differs from the  $G^{\text{tot}}$  CDF, particularly for  $|v| < v_{\text{cont}}$ .

To quantify the deviation of the CDFs from the error function  $\text{erf}$ , we apply the Kolmogorov-Smirnov (KS) test

<sup>1</sup> We consider HZ8 and its “companion” galaxy HZ8W as two distinct sources. We do not consider the quasar HZ5, and the galaxy HZ10 since its [CII] emission line is located at the edge of the observed spectrum.

<sup>2</sup> The value of  $v_{\text{cont}}$  has been chosen in order to minimize the contamination by broad wings. However, its specific value do not affect the results of our study.

<sup>3</sup> A *standard normal deviate* is a random number extracted by a Gaussian distribution having mean equal to zero and standard deviation equal to one.

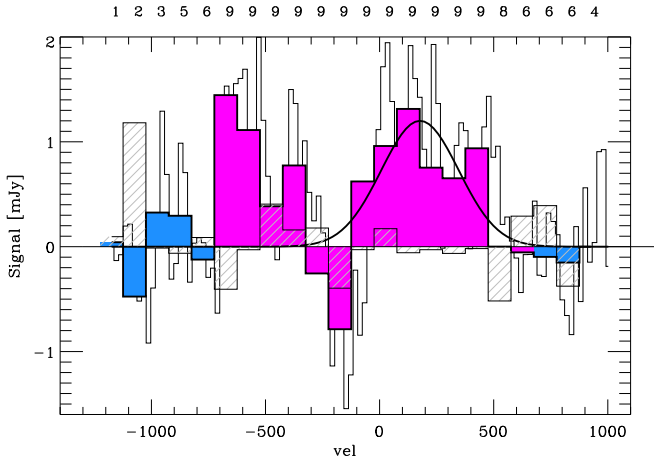


**Figure 2.** The coloured histogram shows  $R^{\text{tot}} \times \bar{\sigma}$ , namely the combined normalized residuals, multiplied for the mean value of the noise of all galaxies. The magenta region refers to pixels characterized by  $|v| < v_{\text{cont}}$ , where  $v_{\text{cont}} = 700 \text{ km s}^{-1}$ , while the blue region represents the region used for the noise determination, namely  $|v| > v_{\text{cont}}$ . The gray hatched histogram represents  $G^{\text{tot}}$ , i.e. the combined Gaussian deviates of mean equal to 0 and standard deviation equal to 1. Both signals have been rebinned to  $100 \text{ km s}^{-1}$ . The thin solid black line shows  $R^{\text{tot}} \times \bar{\sigma}$  at a resolution of  $20 \text{ km s}^{-1}$ . For each spectral bin of the signal we report, on the top of the spectrum, the number of galaxies that contribute to the corresponding flux.

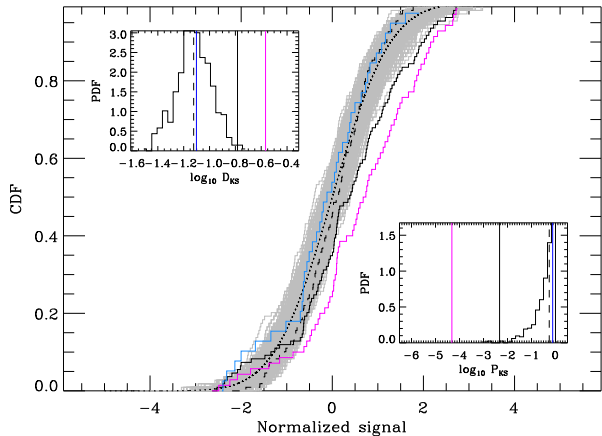


**Figure 3.** Cumulative distribution functions (CDFs) of  $R^{\text{tot}}$  (solid black line) and  $G^{\text{tot}}$  (dashed black line), rebinned to a spectral resolution of  $20 \text{ km s}^{-1}$ . The magenta (blue) line shows the CDF of  $R^{\text{tot}}$  computed in the velocity range  $|v| < v_{\text{cont}}$  ( $|v| > v_{\text{cont}}$ ). The shaded gray region represents the CDFs of 500 *standard normal deviates*, while the dotted line denotes the error function. See the main text for a description of the insets.

to our data. We compute the KS statistics ( $D_{\text{KS}}$ , i.e. the maximum deviation between the CDFs and the *erf*) and the KS probability ( $P_{\text{KS}}$ ) that quantifies the significance level of the KS statistics (small values of the KS probability show that the CDFs are significantly different from the *erf*). We apply the KS test to the CDF of  $G^{\text{tot}}$  and  $R^{\text{tot}}$  and we report the results in Table 1. Moreover, we quantify the deviation

**Table 1.** Results of the Kolmogorov-Smirnov test

	KS statistics	KS probability
$G^{\text{tot}}$	0.07	0.55
$R^{\text{tot}}$	0.16	$5 \times 10^{-3}$
$R^{\text{tot}} ( v  < v_{\text{cont}})$	0.27	$5 \times 10^{-5}$
$R^{\text{tot}} ( v  > v_{\text{cont}})$	0.08	0.76

of the CDFs of the random Gaussian deviates  $G_i$  from the error function *erf*. In the bottom right and top left insets of Fig. 3, we show the probability distribution function (PDF) of  $D_{\text{KS}}^{G_i}$  and  $P_{\text{KS}}^{G_i}$ , respectively, along with the results shown in Table 1. In this case<sup>4</sup>, we find that no Gaussian deviate has a KS statistics as large as 0.16, or equivalently a KS probability as small as  $5 \times 10^{-3}$ .

The residual flux clearly exceeds that of a *standard normal deviates*. We suggest that such excess can be ascribed to broad wings of the [CII] line tracing a starburst-driven outflow. We fit  $R^{\text{tot}} \times \bar{\sigma}$  with a Gaussian characterized by  $F_{\text{peak}} = 1.2 \pm 0.4 \text{ mJy}$ ,  $\text{FWHM} \sim 400 \pm 160 \text{ km s}^{-1}$ , and  $v_0 \sim 177 \pm 68 \text{ km s}^{-1}$ . We note that HZ9, namely the galaxy of our sample characterized by the highest star formation rate ( $\text{SFR} = 67 \text{ M}_{\odot} \text{ yr}^{-1}$ ), contributes almost 20% of the total signal.

### 3 NUMERICAL SIMULATIONS

We test our results against zoomed hydro-simulations of high redshift galaxies performed with the Adaptive Mesh Refinement (AMR) code RAMSES (Teyssier 2002). These simulations will be fully described in Pallottini et al. (2016, in preparation); here, we summarize the aspects of the simulation that are relevant for this work.

Starting from cosmological initial conditions, we carry out a zoom-in simulation of a  $z \sim 7$  dark matter (DM) halo of mass  $\sim 10^{11} \text{ M}_{\odot}$  (virial radius of  $\simeq 15 \text{ kpc}$ ). In the zoomed-in region, the gas mass resolution is  $10^4 \text{ M}_{\odot}$ , and the AMR grid is refined to spatial scales  $\simeq 30 \text{ pc}$ . We form stars from molecular hydrogen, following the model by Krumholz et al. (2009). Stellar feedback includes supernovae, winds from massive stars and radiation pressure (e.g. Agertz et al. 2013). We model the thermal and turbulent energy content of the gas according to the prescriptions by Agertz & Kravtsov (2015). We account for stellar energy inputs and yields that depend both on time and stellar populations (e.g. Kim et al. 2014).

At  $z \sim 7$ , the DM halo hosts a galaxy (named *Dahlia*) characterized by a stellar mass  $M_* \sim 10^{10} \text{ M}_{\odot}$  and a  $\text{SFR} \sim 100 \text{ M}_{\odot} \text{ yr}^{-1}$ . In the top panels of Fig. 4, we show a slice of the density and metallicity fields (left and right, respectively) along with the velocity field orthogonal to the line of sight. Within a radial distance  $r \lesssim 5 \text{ kpc}$  from *Dahlia*'s center, the gas has an average density of  $n \simeq 10 \text{ cm}^{-3}$ , it is enriched to  $Z \simeq 10^{-1} Z_{\odot}$ , and rotates with a velocity  $v_c \sim 100 \text{ km s}^{-1}$ . At  $5 \lesssim (r/\text{kpc}) \lesssim 15$ , *Dahlia* is surrounded by a bubble of low density ( $n \simeq 10^{-1} \text{ cm}^{-3}$ ), low metallicity

<sup>4</sup> We have also applied the Anderson-Darling test to the data finding similar results.

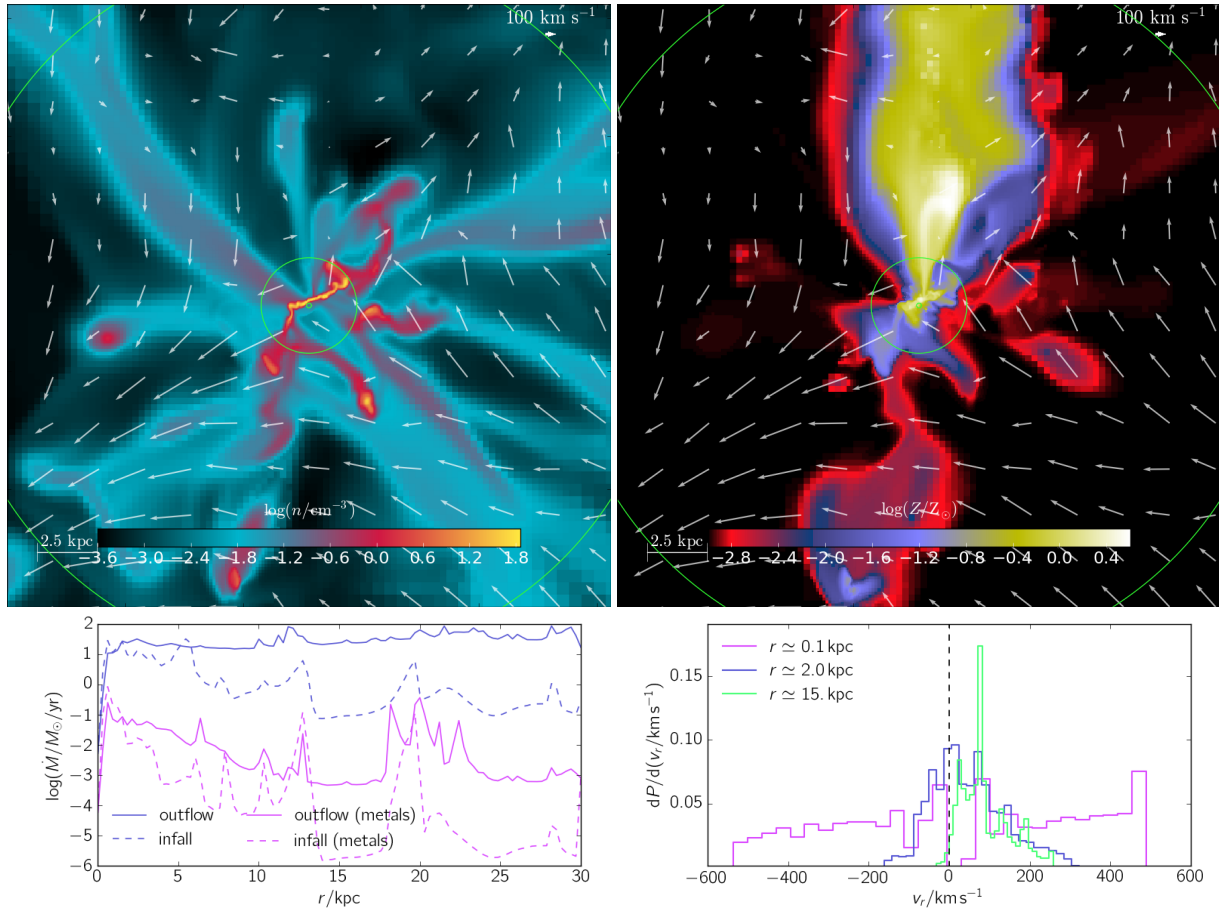


**Figure 4.** Slice of the density ( $n/\text{cm}^{-3}$ , **upper left panel**) and metallicity ( $Z/Z_\odot$ , **upper right panel**) fields centered on the simulated galaxy *Dahlia*. In both maps, the velocity field orthogonal to the line of sight is overplotted with white arrows and the spatial scale is indicated in the lower left corner. Green circles indicate a distance of  $r/\text{kpc} \simeq 0.1, 2, 15$  from the center. The **lower left panel** shows the radially averaged outflow (solid line) and infall (dashed line) rate profiles for the the gas (blue) and metals (magenta). The **lower right panel** shows the PDF of the radial velocity ( $v_r$ ) calculated for the gas at distance  $r \simeq 0.1$  kpc (magenta),  $r \simeq 2$  kpc (blue),  $r \simeq 15$  kpc (green).

( $Z \simeq 10^{-2}Z_\odot$ ) gas, outflowing at a speed  $v \sim 100 \text{ km s}^{-1}$ . In the same region, dense ( $n \simeq 1\text{cm}^{-3}$ ) and almost metal free  $Z \simeq 10^{-3}Z_\odot$  filaments are infalling with a velocity  $v \sim 100 \text{ km s}^{-1}$ . These filaments penetrate *Dahlia*'s circumgalactic medium at a distance of  $\sim 7$  kpc (half of the virial radius), mixing with such component and becoming progressively more isotropic.

To better quantify our analysis, we compute the mass flow rate<sup>5</sup> ( $\dot{M}$ ) and the PDF of the radial velocity ( $v_r$ ) at distances  $r \simeq 0.1$  kpc,  $r \simeq 2$  kpc and  $r \simeq 15$  kpc. The results are shown in Fig. 4, in the bottom left and right panels, respectively.

At the center ( $r \simeq 0.1\text{kpc}$ ), we find high radial velocities ( $\sim 500 \text{ km s}^{-1}$ ) for both the infall and outflow. As the infall fuels gas directly at the center, *Dahlia*'s SFR is mostly concentrated around  $r \simeq 0.1$  kpc. Via stellar feedback, this in turn causes high outflows velocities. Within

$r \simeq 2$  kpc the mass inflow and the outflow rate are nearly equal ( $\sim 30 M_\odot \text{ yr}^{-1}$ ). Interestingly, the two rates are roughly equal also for metals. We interpret this as a result of efficient turbulent mixing between the two flows.

For  $r \gtrsim 2$  kpc the velocity depends only mildly on radius, and since the density is approximately  $\rho \propto r^{-2}$ , the observed constancy of the outflow rate is mostly a consequence of a geometrical effect.

At  $r \gtrsim 5$  kpc, the infall rate drops by a factor  $\gtrsim 10$  below the outflow rate. This is caused by the different spatial structure of the two flows: while the incoming gas rains onto *Dahlia* along narrow filaments, the outflow is essentially spherically symmetric. Note that the outflow is  $\sim 10$  times more enriched than the infall, as most of the gas is essentially of pristine composition. The ratio mildly declines with radius because of the progressive dilution of the outflow metal content with the IGM. The presence of peaks at  $r \sim 12$  kpc and  $r \sim 20$  kpc is due to the presence of satellite galaxies.

<sup>5</sup> The mass flow rate at a distance  $r$  is defined as the material crossing a sphere of radius  $r$ :  $\dot{M} = \int \rho \mathbf{v} \cdot d\mathbf{A}$ , where  $d\mathbf{A}$  is the surface area element,  $\rho = \mu m_p n$  is the proton mass, and  $v_r < 0$  for infalling gas and  $v_r > 0$  for outflowing gas.

## 4 CONCLUSIONS

We have analyzed the [CII] emission lines obtained with ALMA (Capak et al. 2015) in a sample of 9 star-forming ( $5 \lesssim \text{SFR} \lesssim 70 M_{\odot} \text{ yr}^{-1}$ ) high- $z$  ( $5.2 \lesssim z \lesssim 5.7$ ) galaxies. We have fitted each [CII] emission line with a Gaussian function and we have computed the residual by subtracting the best fitting model from the data. By combining the residuals of all the galaxies, we have found a flux excess that can be ascribed to broad wings of the [CII] line tracing a starburst-driven outflow. In order to get a rough estimate of the outflow rate  $\dot{M}$ , we use the following equation:

$$\dot{M} = v_{\text{outfl}} \frac{M_{\text{outfl}}}{R_{\text{outfl}}}, \quad (3)$$

where  $M_{\text{outfl}} \sim 3 \times 10^8 M_{\odot}$  (from eq. 1 by Maiolino et al. 2012) and  $v_{\text{outfl}} \sim 170 \text{ km s}^{-1}$ . For what concerns  $R_{\text{outfl}}$ , we assume that the spatial extent of the outflow is of the order of the radius of the deconvolved [CII] emission sizes, namely  $\sim 1.9 \text{ kpc}$ , a value consistent with the half-light radii of  $z \sim 6$  LAEs (Takatoshi, Masami & Yuichi 2015; Malhotra et al. 2011; Taniguchi et al. 2009). Through this procedure, we tentatively infer an outflow rate of  $\dot{M} \sim 65 M_{\odot} \text{ yr}^{-1}$ , that translates into an average loading factor of  $\sim 2$ , consistent with the ones found in local starbursts (Heckman et al. 2015). We underline, that we are considering for the outflow velocity the shift of the flux excess ( $v_0$ ), that is generally interpreted as the mean velocity of the outflow, while the maximum velocity can be computed as  $v_{\text{max}} = v_0 + \text{FWHM}/2.35 \sim 344 \text{ km s}^{-1}$ . Recently, Heckman & Borthakur (2016) have analyzed a sample of low- $z$  ( $0.2 \lesssim z \lesssim 0.7$ ) galaxies characterized by a large range of SFRs ( $10^{-2} \lesssim \text{SFR}/[M_{\odot} \text{ yr}^{-1}] \lesssim 10^3$ ), and found a strong correlation between the specific SFR (sSFR=SFR/ $M_{\star}$ ) and  $v_{\text{max}}$  (see bottom left panel of their Fig. 1). From their scaling relation, we expect  $v_{\text{max}} \sim 500 \text{ km s}^{-1}$  for a sSFR  $\sim 3 \times 10^{-9} \text{ yr}^{-1}$ , that, given the dispersion in the data and the uncertainties of our estimates are consistent with our findings.

We test these results against state-of-the-art hydrodynamical simulations of *Dahlia*, a star forming (SFR  $\sim 10^2 M_{\odot} \text{ yr}^{-1}$ )  $z \sim 6$  galaxy. Star formation in the simulations is regulated by stellar feedback as radiation pressure and stellar winds from massive stars, and supernovae explosions. We find that, at a distance  $r \lesssim 5 \text{ kpc}$  from the *Dahlia* center, the infall rate is balanced by outflowing gas with  $\dot{M} \sim 30 M_{\odot} \text{ yr}^{-1}$ . At larger distances, the outflow rate remains almost constant, while infalls are characterized by  $\dot{M} \sim 1 M_{\odot} \text{ yr}^{-1}$ .

The simulation outcomes are consistent with our interpretation of the ALMA data suggesting that starburst-driven outflows are in place in the EoR. However, we warn here that we are comparing an observed signal stacked from 9 galaxies with a single synthetic galaxy. For a more specific comparison, we urge to get deeper observations of the [CII] line in the galaxies of this sample to better characterize stellar feedback at high- $z$  and to understand its role in shaping early galaxy formation.

## REFERENCES

Agertz O., Kravtsov A. V., 2015, ApJ, 804, 18

- Agertz O., Kravtsov A. V., Leitner S. N., Gnedin N. Y., 2013, ApJ, 770, 25
- Bouwens R. J., Illingworth G. D., Oesch P. A., Caruana J., Holwerda B., Smit R., Wilkins S., 2015, ApJ, 811, 140
- Bouwens R. J. et al., 2014, ApJ, 793, 115
- Capak P. L. et al., 2015, Nature, 522, 455
- Choudhury T. R., Ferrara A., 2007, MNRAS, 380, L6
- Cicone C. et al., 2015, A&A, 574, A14
- Cicone C. et al., 2014, A&A, 562, A21
- Davé R., Finlator K., Oppenheimer B. D., 2012, MNRAS, 421, 98
- Dayal P., Ferrara A., Dunlop J. S., Pacucci F., 2014, MNRAS, 445, 2545
- Dekel A., Silk J., 1986, ApJ, 303, 39
- D’Odorico V. et al., 2013, MNRAS, 435, 1198
- Dunlop J. S., 2013, in Astrophysics and Space Science Library, Vol. 396, The First Galaxies, Wiklind T., Mobasher B., Bromm V., eds., p. 223
- Feruglio C. et al., 2015, A&A, 583, A99
- Finkelstein S. L. et al., 2012, ApJ, 758, 93
- Hopkins P. F., Quataert E., Murray N., 2012, MNRAS, 421, 3522
- Kim J.-h. et al., 2014, ApJS, 210, 14
- Krumholz M. R., McKee C. F., Tumlinson J., 2009, ApJ, 693, 216
- Lehnert M. D., Heckman T. M., Weaver K. A., 1999, ApJ, 523, 575
- Leitherer C., Ortiz Otálvaro P. A., Bresolin F., Kudritzki R.-P., Lo Faro B., Pauldrach A. W. A., Pettini M., Rix S. A., 2010, ApJS, 189, 309
- Mac Low M.-M., Ferrara A., 1999, ApJ, 513, 142
- Maiolino R. et al., 2012, MNRAS, 425, L66
- Martin C. L., Kobulnicky H. A., Heckman T. M., 2002, ApJ, 574, 663
- Mitra S., Choudhury T. R., Ferrara A., 2012, MNRAS, 419, 1480
- Mitra S., Choudhury T. R., Ferrara A., 2015, MNRAS, 454, L76
- Murray N., Ménard B., Thompson T. A., 2011, ApJ, 735, 66
- Oppenheimer B. D., Davé R., 2006, MNRAS, 373, 1265
- Pallottini A., Ferrara A., Gallerani S., Salvadori S., D’Odorico V., 2014, MNRAS, 440, 2498
- Pallottini et al., 2016, in preparation, 0, 0
- Robertson B. E., Ellis R. S., Furlanetto S. R., Dunlop J. S., 2015, ApJL, 802, L19
- Shapley A. E., Steidel C. C., Pettini M., Adelberger K. L., 2003, ApJ, 588, 65
- Steidel C. C., Erb D. K., Shapley A. E., Pettini M., Reddy N., Bogosavljević M., Rudie G. C., Rakic O., 2010, ApJ, 717, 289
- Teyssier R., 2002, A&A, 385, 337
- Veilleux S., Cecil G., Bland-Hawthorn J., 2005, ARA&A, 43, 769
- Veilleux S. et al., 2013, ApJ, 776, 27
- Walter F., Weiss A., Scoville N., 2002, ApJL, 580, L21